Tracing the *in vivo* fate of nanoparticles with a "non-self" biological identity

Hossein Mohammad-Beigi[1], Carsten Scavenius[2], Pia Bomholt Jensen[1], Kasper Kjaer-Sorensen[2], Claus Oxvig[2], Thomas Boesen[1], Jan J. Enghild[2], Duncan S. Sutherland[1] and Yuya Hayashi[2,*]

[1] *iNANO Interdisciplinary Nanoscience Center, Aarhus University, 8000 Aarhus C, Denmark*

[2] *Department of Molecular Biology and Genetics, Aarhus University, 8000 Aarhus C, Denmark*

* Corresponding author: Yuya Hayashi (yuya.hayashi@mbg.au.dk)

Abstract

A central paradigm in pattern recognition is self/non-self discrimination that remains largely unknown in the light of biological identities nanoparticles acquire *in vivo* and *in vitro*. Using zebrafish embryos as an *in vivo* model for real-time and ultrastructural imaging, here we unravelled the fate of intravenously injected SiO_2 nanoparticles with a "non-self" biological identity. The non-selfness stems from species differences of pre-formed protein corona, and the corona can withstand exposure to blood giving an opportunity for *in vivo* tracing *via* fluorescent tags. Strikingly rapid sequestration and endolysosomal acidification of the nanoparticles in scavenger endothelial cells entailed loss of blood vessel integrity and inflammatory activation of macrophages over time. As the equivalent dose of non-self proteins alone failed to induce the observed pathophysiology, this signifies how the corona enriched with a differential repertoire of proteins can determine the fate of nanoparticles *in vivo*.

Exploitation of "self" molecules at nanoparticles for biomimetic camouflage is a strategy for prolonging the circulation half-life to target tumours *in vivo*[1-3]. The biological identity of nanoparticles *in vivo* is, in a way, understood as altered self because it originates from the corona of self biomolecules interacting with nanoparticles in a natural non-specific manner[3-6]. Proteins, among other biomolecules, are of particular interest as they can take "unnatural" shapes at the nanoparticles potentially exposing their cryptic epitopes with unexpected biological consequences[7,8]. Only little is known, however, about how the protein corona (PC) is recognized within the canonical regime nature has devised to combat pathogens and for self-maintenance. Non-self detection in innate immunity relies on the complement system and pattern recognition of conserved motifs associated with pathogens/danger signals at the cellular level[9]. The PC as a non-self biological identity could be interpreted as local enrichment of potentially immunogenic (foreign) proteins[10] and (surface-)induced conformational changes of these proteins[7,8] that may expose yet another epitopes for pattern recognition machineries. Despite the prevailing idea of the

biological identity, only a few *in vitro* studies have tested the mismatching combination of fetal bovine serum (FBS) and (transformed) human/murine cell lines[11-13] or zebrafish primary blood cells[14]. While these studies highlight altered cellular interaction of nanoparticles by the PC of different species origin, to our knowledge, none has addressed how the non-self biological identity determines the fate of the nanoparticles *in vivo*.

Zebrafish embryos have recently emerged as a bioimaging model for preclinical screening of nanomedicines[15-23] with a unique opportunity of whole-embryo fixation for transmission electron microscopy (TEM) to visualize intracellular trafficking of nanoparticles *in vivo* at high resolution[24,25]. Here we used the zebrafish model to unravel the *in vivo* journey of 70 nm SiO_2 nanoparticles with pre-formed FBS PC and the pathophysiological consequences. The nanoparticles represent a model system especially suited for this study owing to the matrix-incorporated fluorescence tracers of choice, intrinsic high electron density of SiO_2, and the large particle size that allows excellent recovery of the nanoparticle-protein complexes even after extensive washing by centrifugation. We have previously established an intravital real-time imaging approach for the same SiO_2 nanoparticles but without pre-formed FBS PC (hereafter referred to as "Pristine nanoparticles")[25]. Of note is the scavenger phenotype of venous endothelial cells (ECs) lining the caudal vein (CV) and the CV plexus, the functional analogue of liver sinusoidal ECs in mammals[16], which continuously sequestered blood-borne nanoparticles in a scavenger receptor-dependent manner[25] with blood clearance kinetics resembling that of mammalian models[26]. Macrophages, on the other hand, engaged blood-borne nanoparticles rapidly *via* membrane adhesion and constitutive macropinocytosis independently of scavenger receptors and without pro-inflammatory responses[25]. The assumption here is that Pristine nanoparticles, like in other *in vivo* experimentation, acquire a self biological identity as soon as they are introduced to the bloodstream[27] whilst pre-formed FBS PC retains its compositional profile until localized intracellularly. By tracing the *in vivo* fate of the non-self biological identity, we find rapid nanoparticle sequestration and strong induction of pro-inflammatory responses within a time-scale from minutes to several hours.

Exposure to blood plasma proteins does not overwrite but add to the protein corona pre-formed of FBS.

A critical premise for testing non-self biological identities *in vivo* is retention of the pre-formed FBS PC until eventually cleared from the bloodstream. We started with characterizing 70 nm SiO_2 nanoparticles of three different surface types (Plain, NH_2 and COOH) with or without pre-formed FBS PC. For the formation of FBS PC, the nanoparticles were mixed in 90% (v/v) heat-inactivated FBS and washed by multi-step centrifugation as previously described[14]. The FBS PC nanoparticles thus prepared display a colloidally stable population (Fig. 1a,b and Supplementary Fig. 1) with an average size increase of ~30 nm in hydrodynamic diameter for the plain surface and even larger (~50 nm) for NH_2 and COOH surfaces (Supplementary Table 1).

To study the retention of FBS PC *in vitro*, we used zebrafish blood plasma (DrBP) harvested from adult male fish[14] as a substitute for an *in vivo* blood protein repertoire. It should be noted, however, that the liver of the zebrafish embryos at 3 days post-fertilization (dpf) is not fully functional for protein production and therefore the plasma proteome in adult fish[28] does not entirely reflect the native protein repertoire at this embryonic stage[29]. As discussed previously[14], the plasma protein repertoires of mammals and zebrafish are well conserved except for the absence of serum albumin in the latter[30]. These differences would form the basis of the non-self biological identity of FBS PC nanoparticles. To first identify proteins with a high affinity for the nanoparticles, PC purely made of FBS or DrBP was analyzed by SDS-PAGE and tandem mass spectrometry (MS/MS) for protein identification. While Fetuin-A was specifically enriched in DrBP PC, Apoa1 and Apoa2 were two common proteins that constitute a major component of FBS PC and DrBP PC (Fig. 1c and Supplementary Fig. 2) confirming the previous results[14]. Notably, nanoparticles with the COOH surface showed PC profiles skewed towards high molecular weight proteins for both of FBS PC and DrBP PC, and those with the NH_2 surface had closer PC profiles to plain surface nanoparticles (Supplementary Fig. 3).

Next, we have chosen 15 min as the minimal duration for the incubation of FBS PC nanoparticles in DrBP to characterize PC retention *in vitro*, corresponding to previously estimated elimination half-life of 14 min following IV injection of the same SiO_2 nanoparticles but without pre-formed FBS PC[25]. Fluorescence labelling and MS/MS approaches confirmed retention of APOA1 in the FBS PC while Fetuin-A was added from the 15 min incubation in DrBP (Fig. 1d,e and Supplementary Figs. 2 and 4). This was particularly well observed with the plain surface, where only 7% reduction in proteins of FBS origin was evident with 29% being additional proteins acquired from DrBP after 15 min incubation (Fig. 1f,g). The other two surface types had 9% reduction of FBS PC especially in the high molecular weight range but attracted even greater amounts of DrBP representing close to or more than the half of the "mixed" identity of the newly formed PC (Fig. 1g, and Supplementary Figs. 2 and 4). These results need to be interpreted with caution, because in addition to the anticipated difference of the plasma proteomes as described above, the spontaneous formation of PC *in vivo* tends to display more diverse arrays of proteins than the counterpart *ex vivo* PC in mice[5] and in humans[6]. The *in vivo* milieu of bloodstream rich in biomolecules and other biological entities could thus competitively replace a certain fraction of the pre-formed PC (as a non-self biological identity) as fast as 5 min post-injection (mpi) in mice, although unclear in the quantity[31]. For our purpose is to maximally retain the non-self biological identity as of the pre-formed PC, we selected plain surface nanoparticles for further studies on the basis of the minimal addition of blood proteins *in vitro*. Interestingly, prolonged exposure to DrBP (6 h) resulted in a decrease of the Fetuin-A content but an increase the Apoa1:APOA1 ratio indicating exchange of the same type of proteins that differ in the species origin (Supplementary Figs. 2 and 5).

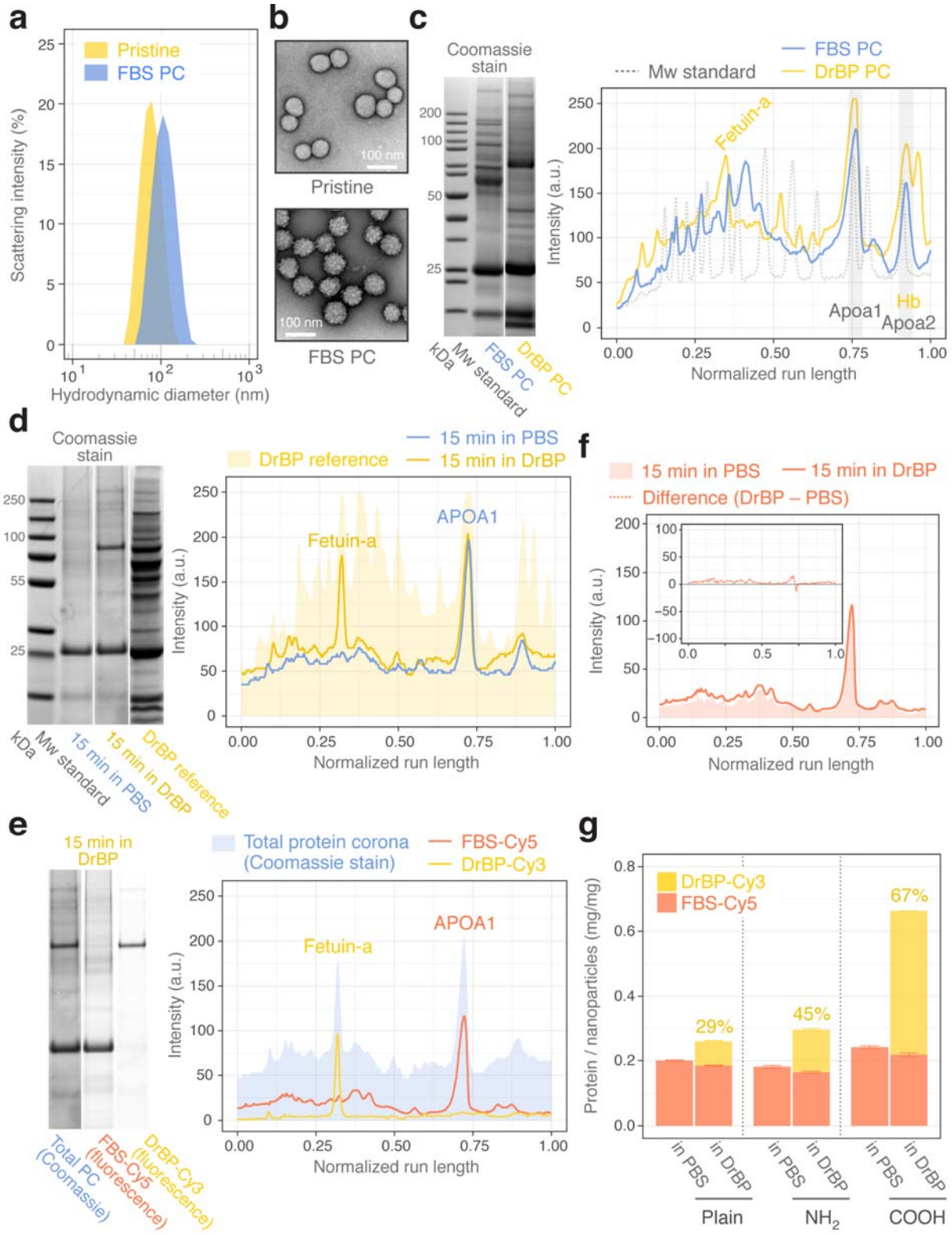

Figure 1. Characterization of FBS PC nanoparticles and retention of the PC *in vitro*. a, DLS analysis on the hydrodynamic size distribution verifying a stable dispersion of FBS PC nanoparticles. **b,** TEM images of negatively-stained SiO_2 nanoparticles. FBS PC nanoparticles

show globular appearance of dehydrated proteins at nanoparticles. Scale bars, 100 nm. **c,d,** SDS-PAGE profiles of Coomassie Brilliant Blue-stained corona proteins (nominal mass of nanoparticles loaded: 150 µg in **c**, 30 µg in **d**). FBS PC is compared against DrBP PC to reveal proteins with an intrinsically high affinity for the SiO_2 nanoparticles (**c**). Incubation of FBS PC nanoparticles in DrBP (see "DrBP reference" for the total protein repertoire) adds further proteins to the existing FBS PC (**d**). Selected bands were excised for MS/MS protein identification and the peaks annotated in the profile plot. Note Apoa1 was identified previously[14] and thus excluded from analysis in this study. Shaded peaks and grey-coloured annotations indicate proteins common to FBS and DrBP. Original gel images and details of identified proteins are shown in Supplementary Fig. 1. **e,** Fluorescence scans distinguish the origins of the two highly enriched corona proteins, which were further validated by MS/MS protein identification. **f,** SDS-PAGE profiles of FBS-Cy5 reveal no particular removal of FBS PC even following 15 min incubation in DrBP. **g,** Fluorimetry-based quantification of FBS-Cy5 and DrBP-Cy3 in the PC. Two other surface types of 70 nm SiO_2 nanoparticles are included (NH_2 and COOH functionalized; see Supplementary Figs. 1-4 for all characterization results). The percentages shown above the columns are the fraction of DrBP in the total PC. Values are mean ± s.d. of two measurements. a.u., arbitrary units.

Nanoparticles with a pre-formed FBS protein corona are rapidly sequestered.

As previously[25], nanoparticles with pre-formed FBS PC were IV injected at the common cardinal vein that leads to similar biodistribution as that of Pristine but with extended sequestration in veins (Fig. 2a and Supplementary Fig. 6). Nearly complete blood clearance was observed already at 1 hpi (Supplementary Fig. 6), and thus we performed time-lapse imaging up to 30 mpi at ROI (see Fig. 1a) to resolve the rapid sequestration kinetics (Movies 1 and 2). The nanoparticle concentration in the bloodstream was clearly lower for FBS PC nanoparticles, as determined by the mean fluorescence intensity (FI) in the caudal artery (CA), with a larger exponential decay function than that of Pristine nanoparticles (Fig. 1b-d). Nanoparticle sequestration was also strikingly faster for FBS PC nanoparticles initiated with massive adherence to scavenger ECs rather than macrophages (Fig. 1b,c,e). This underscores contrasting mechanisms for immediate membrane associations of the Pristine and FBS PC nanoparticles by which macrophages and scavenger ECs, respectively, play the dominant role within minutes after IV injection (ref[25] and Fig. 1).

The signals from sequestered FBS PC nanoparticles (NP-FITC) in scavenger ECs, however, did not continue to increase (Fig. 1c,e) despite the consistent accumulation of FBS-Cy5 representing FBS PC (Fig. 1c,f). This can be explained by pH-dependent quenching of FITC incorporated into the SiO_2 matrix of the nanoparticle core, as a result of which >50% of NP-FITC fluorescence is lost at lysosomal pH of 4.7 while FBS-Cy5 is little affected both as a label for free proteins and PC (Supplementary Fig. S7). Pacific Blue, on the other hand, has pK_a of 3.7 and proved its stability in acidic organelles in live cells[32] as well as zebrafish embryos in our previous report[25]. As it is prone to photobleaching, we opted for imaging at two time points (3 and 24 mpi) on a different set of embryos to calculate relative changes from 3 mpi. FBS PC nanoparticles (Pacific Blue) were thus prepared likewise to complement the FITC dataset. Estimated values based on the relative proportions are plotted along with the time-lapse results, validating the kinetics for blood clearance (Fig. 1d) and FBS PC accumulation (Fig. 1f) and indicating how the total FI for sequestered nanoparticles would have increased if FITC was not quenched (Fig. 1e). FBS PC

nanoparticles were rapidly cleared from the bloodstream at a faster rate than that of Pristine nanoparticles, and this rapidity seems contributed by specific interactions with scavenger ECs rather than macrophages. The non-self biological identity represented by FBS PC nanoparticles was also significantly more accumulated than the male DrBP counterpart *in vitro* by blood cells harvested from adult zebrafish[14]. It would therefore be interesting to identify at the molecular level what surface receptors are possibly involved in the rapid sequestration process and if they are a common feature between scavenger ECs and blood cells at later stages of development.

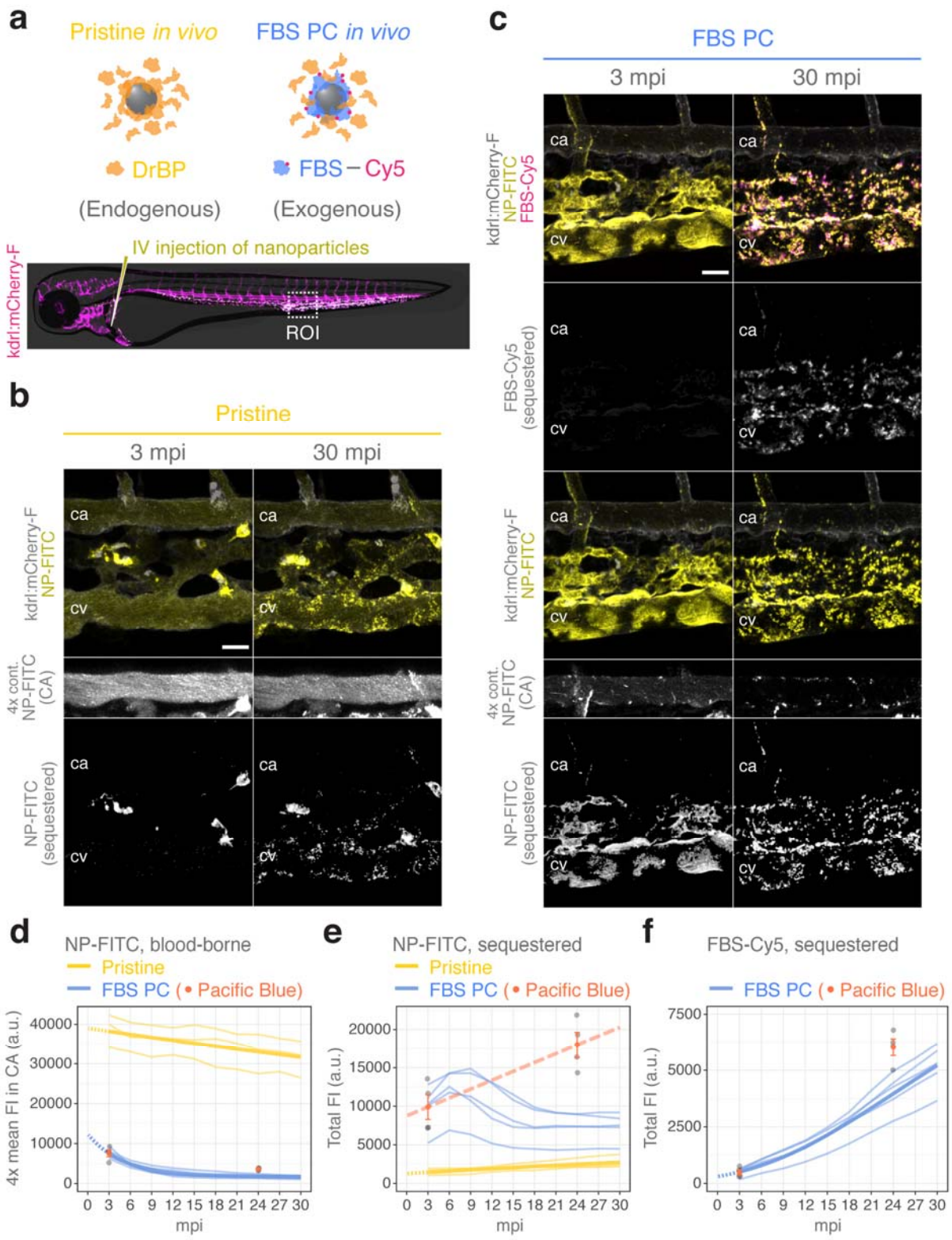

Figure 2. *In vivo* imaging of FBS PC nanoparticle sequestration. a, Schematics representing the expected PC profiles for Pristine and FBS PC nanoparticles in the *in vivo* setting. The panel below depicts the blood vessel networks in the 3 dpf embryo labelled by mCherry with an overlaid

illustration of the whole embryo to guide the site of IV injection and ROI. See Supplementary Fig. 6 for the original images showing biodistribution of the injected nanoparticles. **b-f,** *Tg(kdrl:mCherry-F)* embryos at 3 dpf were injected with FITC-labelled SiO_2 nanoparticles (NP-FITC) with or without pre-formed FBS PC (FBS-Cy5) and imaged every 3 min starting from 3 mpi. Representative images showing sequestration of Pristine (**b**) and FBS PC (**c**) nanoparticles. The huge clusters of nanoparticles found in **b** are likely those associated with macrophages[25]. The NP-FITC signals in the CA are multiplied by 4-fold to aid visualization. Anterior left, dorsal top. Scale bars, 20 µm. Kinetics for clearance of blood-borne nanoparticles (**d**) and sequestration of nanoparticles (**e**) and FBS PC (**f**) are plotted as individual embryos (thin lines, n = 3 for Pristine, n = 5 for FBS PC) and, where possible, curve-fitted (thick lines). Dashed lines between 0-3 mpi are predictions from the fitted models. Results from Pacific Blue-labelled SiO_2 nanoparticles are plotted for the two time points as individual embryos (grey points, n = 4) and as the mean ± s.e.m. (orange-coloured). Note that the values are estimated from the relative difference between 3 and 24 mpi, where the mean values at 3 mpi are the same for FITC-labelled and Pacific Blue-labelled nanoparticles. Linear fitting (the long-dashed line) is shown in **e**. a.u., arbitrary units. See Movies 1 and 2 for the time-lapse sequences.

The protein corona undergoes acidification after endolysosomal sequestration.

To verify that the loss of NP-FITC fluorescence was caused by endolysosomal acidification following nanoparticle uptake, we have devised a dual labelling strategy by which the fluorescence ratio of pHrodo (pH indicator) to Cy5 (pH insensitive) responds to local acidification within a cell. The fluorescence response of the dyes as a label for free proteins and nanoparticle-protein complexes to the pH range relevant for endosomes (pH 5.5-6.3) and lysosomes (pH 4.7)[33] confirmed the positive correlation between acidification and increase in the pHrodo/Cy5 ratio (Fig. 3a and Supplementary Fig. 7). We then quantified the fluorescence ratio using a 3D mask approach[25] whereby the colocalization of Cy5 and pHrodo signals was determined at each focal plane of 2 µm-thick optical sections before maximum intensity projection of a stacked image. The ratio was calculated within the projected image at each pixel in the 32-bit float mode and the median value was obtained. The increase in the pHrodo/Cy5 ratio was clearly visible between 6 to 12 mpi (Fig. 3b and Movie 3) but the largest change was in fact estimated to be occurring at 5 mpi (Fig. 3c) in line with the lysosomal acidification kinetics[34]. We observed the same pattern when we simply calculated the fluorescence ratio using median values from each signal channel (data not shown) and when we used Pacific Blue nanoparticles for the two time points (Fig. 3c).

At the ultrastructural level, FBS PC nanoparticles were singly dispersed in the blood lumen, internalized *via* endocytosis, and sequestered in endolysosomal compartments in scavenger ECs (Fig. 3d) in a similar manner previously observed for Pristine nanoparticles[25]. We were, however, unable to identify macrophages at this time point (30 mpi) unlike the previous study in which macrophages rapidly captured Pristine nanoparticles *via* membrane adherence and macropinocytosis[25]. In contrast to the patchy localization observed for Pristine nanoparticles (Fig. 3e and ref[25]), FBS PC nanoparticles were compartmentalized at a high density (Fig. 3f), as anticipated from the intravital imaging results. The lumen of those endolysosomal compartments observed with FBS PC nanoparticles differed in the electron density giving a light to dark contrast (Fig. 3 f), likely due to acidification of the vesicle[35]. FBS PC nanoparticles thus undergo rapid

cellular sequestration and subsequently experience acidification in the endolysosomal compartments in scavenger ECs. These biological processes we observed here mostly occurred within the first 1 h, and this underscores the importance of resolving early phase kinetics in the *in vivo* setting where rapid blood clearance is frequently reported also in mammalian models[3,26,36].

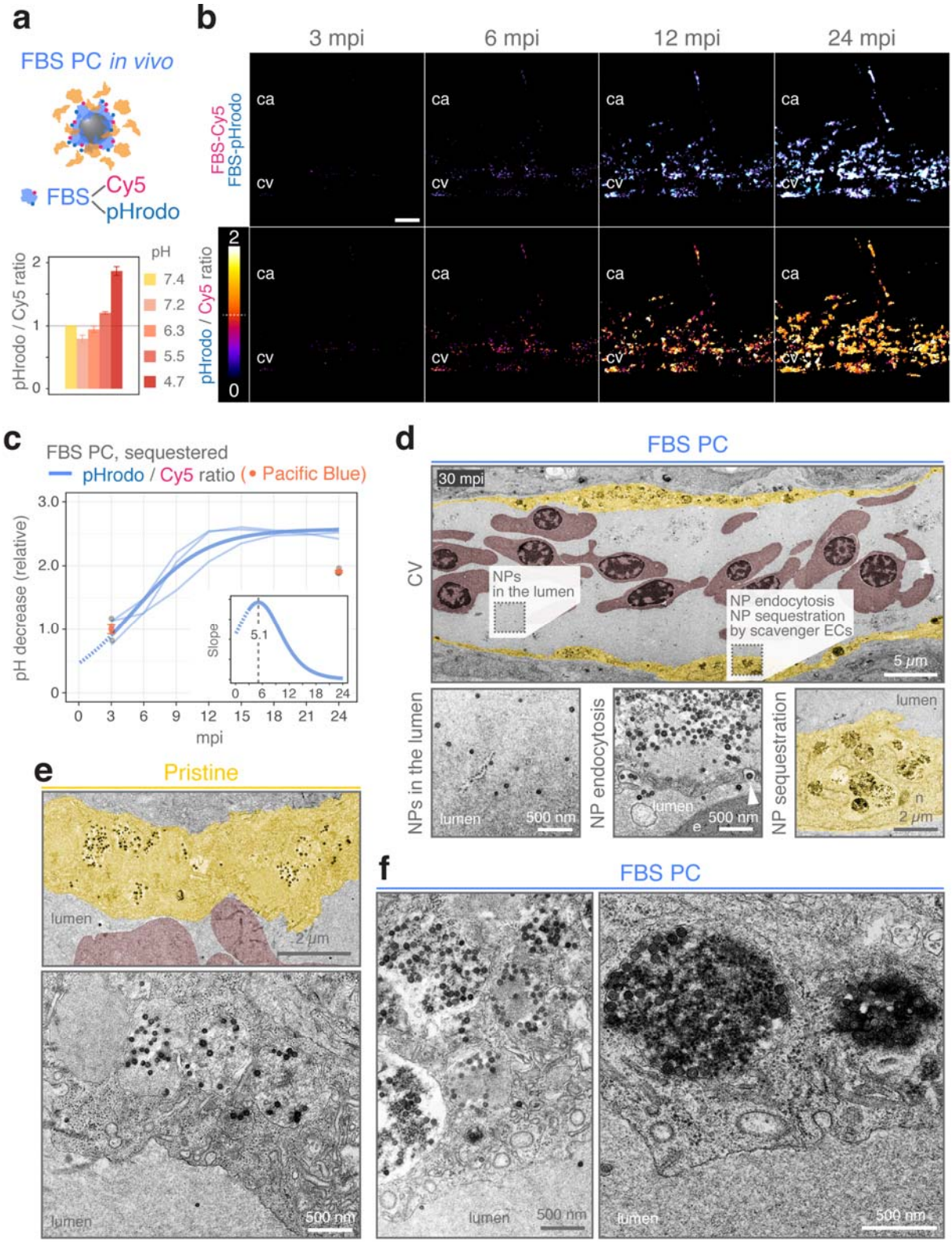

Figure 3. Acidification of FBS PC nanoparticles following endolysosomal sequestration. a, Schematic illustrating dual-labelled FBS PC nanoparticles for quantification of the fluorescence ratio of pHrodo to Cy5. The graph below shows the fluorescence ratio *in vitro* measured by

fluorimetry at the intracellular pH range (mean ± s.d., n = 2), indicating an increase in the ratio at pH 5.5 and 4.7. **b,c,** Wild-type embryos at 3 dpf were injected with FITC-labelled SiO_2 nanoparticles with pre-formed FBS PC (FBS-Cy5 and FBS-pHrodo) and imaged every 3 min starting from 3 mpi. Representative images showing sequestration of dual-labelled FBS PC and the fluorescence ratios, 0-2 scaled (**b**). Anterior left, dorsal top. Scale bars, 20 µm. The median fluorescence ratios are plotted relative to 3 mpi as individual embryos (thin lines, n = 3) and curve-fitted (the thick line) (**c**). The dashed line between 0-3 mpi is prediction from the fitted model. The slope of the fitted curve is shown in the inset with the vertical dashed line indicating the peak maximum. Results from Pacific Blue-labelled SiO_2 nanoparticles are plotted for the two time points as individual embryos (grey points, n = 4) and as the mean ± s.e.m. (orange-coloured). Note that the values are estimated from the relative difference between 3 and 24 mpi, where the mean values at 3 mpi are the same for FITC-labelled and Pacific Blue-labelled nanoparticles. See Movie 3 for the time-lapse sequence. **d-f,** Wild-type embryos at 3 dpf were injected with FITC-labelled SiO_2 nanoparticles with or without pre-formed FBS PC and chemically fixed at 30 mpi for TEM imaging. Representative (tiled) images indicating the observed aspects of particular note (**d**), sequestered Pristine nanoparticles (**e**) and FBS PC nanoparticles frequently found with highly electron-dense vesicular lumen (**f**). In low magnification images, scavenger ECs and erythrocytes are pseudo-coloured in yellow and red, respectively, to visually aid the boundaries between the cells and the blood lumen. NP, nanoparticle. e, erythrocytes. n, nucleus.

The protein corona is degraded over time along with loss of blood vessel integrity and induction of pro-inflammatory responses.

As FBS PC nanoparticles were confined in the endolysosomal pathways, we next determined degradation of the PC by quantifying the fluorescence ratio of FBS-Cy5 to NP-Pacific Blue at selected time-points (1, 2, 4 and 6 hpi). Here we assumed that the two dyes are insensitive to pH changes and thus any decrease in the fluorescence ratio would correlate with disengagement of the PC from nanoparticles. This is achieved by the pixel-by-pixel fluorescence ratio approach that effectively excludes signal contributions from diffused FBS-Cy5 dyes as they would no longer colocalize with NP-Pacific Blue signals. To further assess the fluorescence ratio separately for ECs and macrophages, double transgenic embryos from a combination of respective constitutive reporter lines were used in conjunction with the 3D mask approach for colocalization of FBS PC nanoparticle signals with cell types of interest (Supplementary Fig. 8). The fluorescence ratio was significantly lower for macrophages at 6 hpi (60%) and to a lesser extent for ECs (79%), suggesting the onset of PC degradation to be between 4 and 6 hpi (Fig. 4a-d). All other parameters tested were not significantly different except for an unexpected lower cell area of ECs at 1 hpi (Supplementary Fig. 9). With a surprisingly similar time-course, earlier *in vitro* studies reported lysosomal degradation of PC to occur around 7 h of exposure[37,38].

This time-frame of 4-6 hpi also corresponds to the initiation of FBS-Cy5 fluorescence decay observed in 12 h time-lapse imaging, delivering an estimate of overall 27% reduction from 4 to 6 hpi (Supplementary Fig. 10). However, unlike the fluorescence ratio approach, this kinetics seems also influenced by the physiological state of scavenger ECs. We have noticed that the constitutive reporter signals labelling mainly ECs (*kdrl:mCherry-F*) consistently decreased over time towards 12 hpi of FBS PC nanoparticles, which was much less obvious for embryos injected with water (a vehicle control) or Pristine nanoparticles with a 5-times less decay constant than that for FBS PC nanoparticles (Fig. 4e,f, Movies 4-6 and Supplementary Fig. 10). In stark contrast to the overall decrease of fluorescence signals in the two controls, the scavenger phenotype of ECs (forming the

blood vessels in the CV and CVP but not the CA) was particularly affected as clearly depicted in Fig. 4e and Movie 6. This shows striking similarity to the gradual loss of *kdrl:GFP* signals in scavenger ECs passively targeted by liposomal delivery of a cytotoxic drug resulting in compromised blood vessel integrity[16]. Underscoring the targeted cytotoxicity, the signals from sequestered FBS PC nanoparticles also diminished along with the fading *kdrl:mCherry-F* signals (Fig. 4g and Supplementary Fig. 10), likely an indication for the disintegrated vasculature.

In the subsequent experiment, we used double transgenic *Tg(mpeg1:mCherry); Tg(tnfa:GFP-F)* embryos to determine the pathophysiological consequence by the inducible reporter for transcriptional activation of the pro-inflammatory cytokine *tnfa* (*tumour necrosis factor alpha*)[39]. We first noted an overall decrease in the total cell area of macrophages which was not treatment-specific, suggesting no particular recruitment of macrophages from other parts of the body (Fig. 5a,b). We then quantified the macrophage-specific contribution to the overall FBS PC signals, as the scavenger ECs were critically affected losing their ability as the predominant sink of sequestered FBS PC nanoparticles (Fig. 4e-g). The increasing contribution of macrophages to the overall FBS PC signals (Fig. 5a,c) may explain, although speculative as yet, sweeping of sequestered FBS PC nanoparticles that once belonged to scavenger ECs through phagocytosis of apoptotic/necrotic cell debris[40]. As reported elsewhere[41], the blob-like *kdrl:mCherry-F* signals seen in Fig. 4e represent EC-derived extracellular vesicles (e.g. apoptotic bodies) accumulated by macrophages, and some of the FBS-Cy5 signals indeed began to associate with them displaying a wandering behaviour (see the highly mobile, blob-like signals in Movie 6).

Induction of *tnfa* is a molecular signature of M1-like (inflammatory) polarization in macrophages[39], and this phenotype propagated to ~50% (cell area) of macrophages within the ROI until approximately 6 hpi and persisted towards 12 hpi (Fig. 5d). This observation was specific to FBS PC nanoparticles or the positive control (LPS; lipopolysaccharides), and not to FBS proteins at the equivalent dose, Pristine nanoparticles or water (Movies 7-11). The rate of propagation peaked at 3 hpi for FBS PC nanoparticles and 3.5 hpi for LPS (Fig. 5e), implying involvement of different

stimuli for the activation. It remains unclear, however, whether the pro-inflammatory cascade was initiated by macrophages or scavenger ECs. LPS is known to act as a Toll-like receptor 4-agonist in mammals, but not in zebrafish that exhibit a high tolerance for the endotoxin shock[42] while nonetheless require myeloid differentiation factor 88 (an adaptor for Toll-like receptor signalling axis) in LPS-induced inflammation[43]. In the case of FBS PC nanoparticles, direct recognition of the non-self biological identity presented at the nanoparticles is an interesting possibility, which could in principle be supported by a positive correlation between the FBS PC sequestration in macrophages and pro-inflammatory responses. However, it seems unlikely the case as the M1-like phenotype-specific contribution to the sequestered FBS-Cy5 signals did not propagate (Fig. 5c) and those *tnfa*$^{+}$ macrophages without FBS PC nanoparticles were also identified (Fig. 5a and Movie 10). In contrast, our observation of scavenger EC disintegration at corresponding time-course (Fig. 4) favours a scenario in which extracellular pro-inflammatory stimuli such as damage-associated molecular patterns are involved in this pathophysiological consequence[44,45].

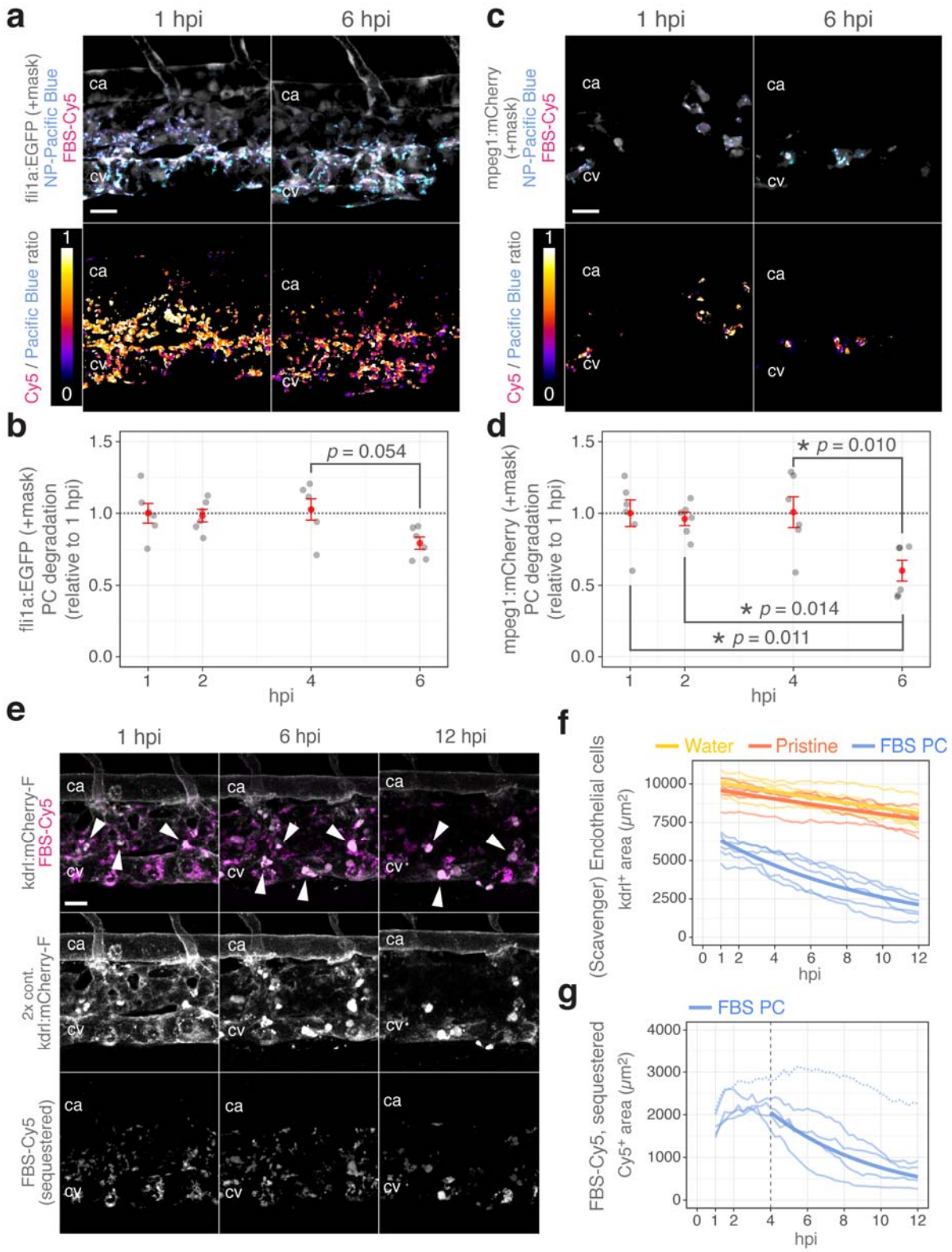

Figure 4. Degradation of PC and loss of blood vessel integrity. a-d, *Tg(fli1a:EGFP); Tg(mpeg1:mCherry)* embryos at 3 dpf were injected with Pacific Blue-labelled SiO_2 nanoparticles (NP-Pacific Blue) with pre-formed FBS PC (FBS-Cy5) for each time point of 1, 2, 4 and 6 hpi and

imaged independently. Representative images showing EC- (**a**) and macrophage-specific (**c**) signals for NP-Pacific Blue and FBS-Cy5 as well as the fluorescence ratios of Cy5 to Pacific Blue, 0-1 scaled. Anterior left, dorsal top. Scale bars, 20 µm. The median fluorescence ratios were plotted relative to 1 hpi for ECs (**b**) and macrophages (**d**) as individual embryos (grey points, n = 6) and the mean ± s.e.m. (red-coloured). Significant differences were tested by one-way ANOVA with Tukey's HSD post-hoc comparisons (degrees of freedom = 20, F values = 3.295 for ECs and 6.066 for macrophages). See Supplementary Figs. 8 and 9 for the details of image analysis. **e-g,** *Tg(kdrl:mCherry-F)* embryos at 3 dpf were injected with FITC-labelled SiO_2 nanoparticles with or without pre-formed FBS PC (FBS-Cy5) and imaged every 15 min starting at 1 hpi. Representative images showing the loss of fluorescence signals from scavenger ECs and sequestered FBS PC. The mCherry signals are multiplied by 2-fold to aid visualization. Arrowheads denote blob-like signals of mCherry (and to some extent, of FBS-Cy5) likely specific to sequestration in macrophages. Anterior left, dorsal top. Scale bars, 20 µm. Areas representing ECs (the mCherry signals, **f**) and sequestered FBS PC (the Cy5 signals, **g**) are plotted over time as individual embryos (thin lines, n = 5) and curve-fitted (thick lines). The curve fitting in **g** was performed after excluding an outlier (the dashed line) and between 4-12 hpi where steady decreases are observed. See Supplementary Fig. 10 for a comparison between Pristine and FBS PC nanoparticles. See Movies 4-6 for the time-lapse sequences.

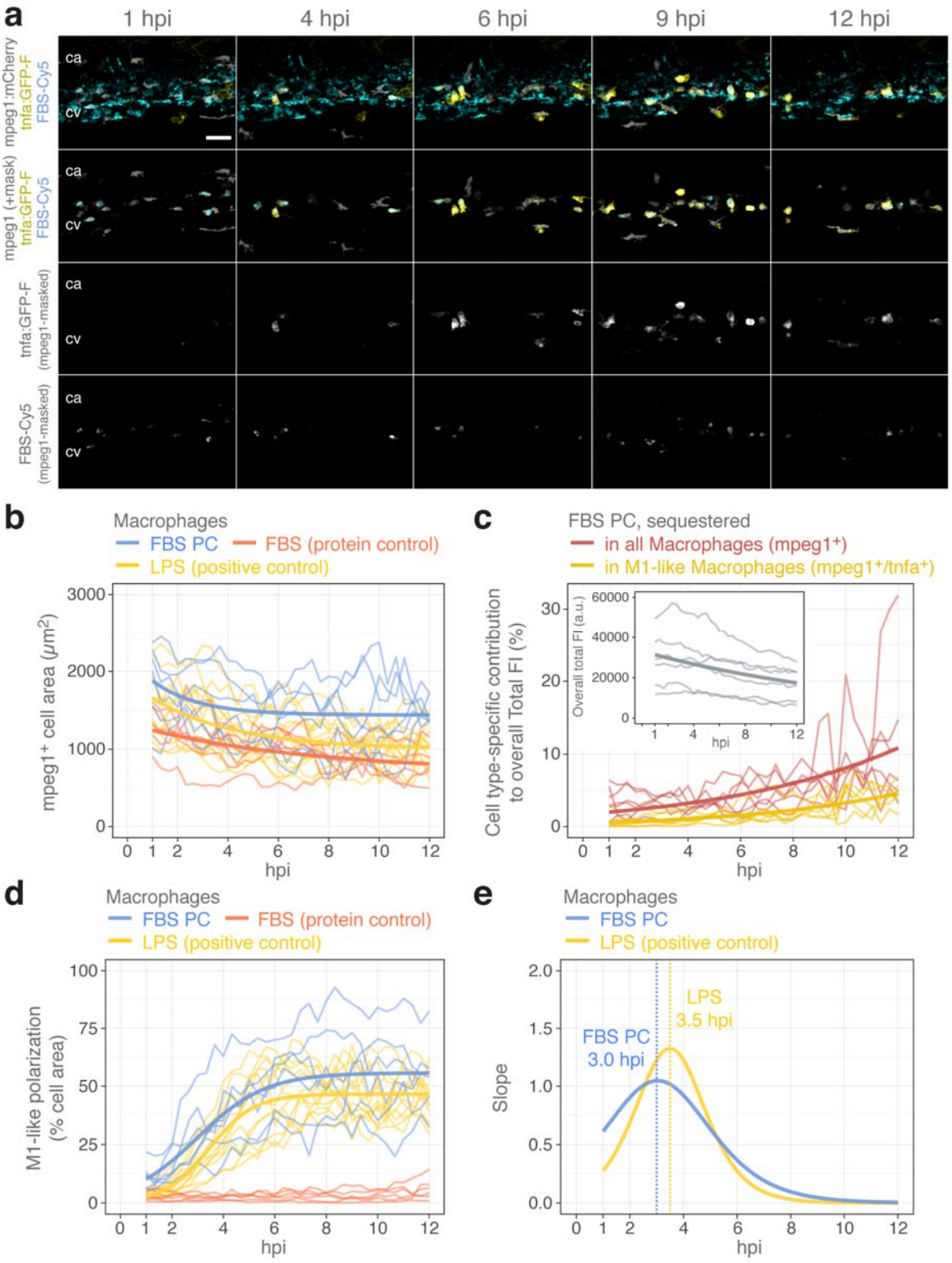

Figure 5. FBS PC nanoparticles induce M1-like polarization of macrophages. a-e, *Tg(mpeg1:mCherry); Tg(tnfa:GFP-F)* embryos at 3 dpf were injected with Pacific Blue-labelled SiO_2 nanoparticles with pre-formed FBS PC (FBS-Cy5), FBS proteins only (at the equivalent

protein mass of FBS PC nanoparticles) or LPS and imaged every 20 min starting from 1 hpi. Representative images showing the time-course of FBS PC sequestration and induction of *tnfa* with or without the macrophage mask. Anterior left, dorsal top. Scale bars, 30 µm. Image analysis results and fitted models are plotted as individual embryos (thin lines, n = 6 for FBS PC nanoparticles and FBS proteins only, n = 12 for LPS) and, where possible, curve-fitted (thick lines). Kinetics are shown for the cell area of macrophages (**b**), cell type-specific contributions to overall sequestration of FBS PC (**c**), the degree of M1-like polarization represented by percentage of colocalized areas between *tnfa*$^+$ and *mpeg1*$^+$ (**d**), and the slopes derived from **d** with vertical dashed lines indicating the peak maxima. a.u., arbitrary units. See Movies 7-11 for the time-lapse sequences including negative results obtained from water control and Pristine nanoparticles.

Conclusions

Here we demonstrated the biological fate of FBS PC nanoparticles and pathophysiological consequences *in vivo* using a multicolour combinations of fluorescent tracers and endogenous reporters labelling ECs, macrophages and their M1-like phenotype in zebrafish embryos. To gain a holistic insight into the *in vivo* journey of the FBS PC, we addressed four aspects covering retention, rapid sequestration, acidification and intracellular degradation of the PC that eventually leads to pro-inflammatory responses (Fig. 6). The sequestration kinetics of the FBS PC nanoparticles was strikingly different from that of Pristine nanoparticles whereby scavenger ECs likely play the predominant role in rapid clearance from the bloodstream. The scavenger ECs were thus heavily loaded with FBS PC nanoparticles and as a consequence the blood vasculature were disintegrated, allowing macrophages to scavenge the cell debris along with sequestered nanoparticles. The inflammatory conditions are further supported by concurrent M1-like polarization of those macrophages with a time-frame of several hours after IV injection. This cannot be explained solely by the immune intolerance to the non-native protein repertoire presented by FBS, as the free proteins at the equivalent dose failed to mimic the pro-inflammatory responses. Although the molecular mechanisms linking the "foreignness" of PC to the observed inflammatory events remain obscured, the non-self biological identity of nanoparticles clearly impacted *in vivo* aspects that are of particular concern in safe-by-design development of nanomedicines such as blood clearance and pathophysiology. Our findings thus provide an experimental *in vivo* proof of the founding concept that the cell "sees" the biological identity[46] to determine a differential fate of the same nanoparticles.

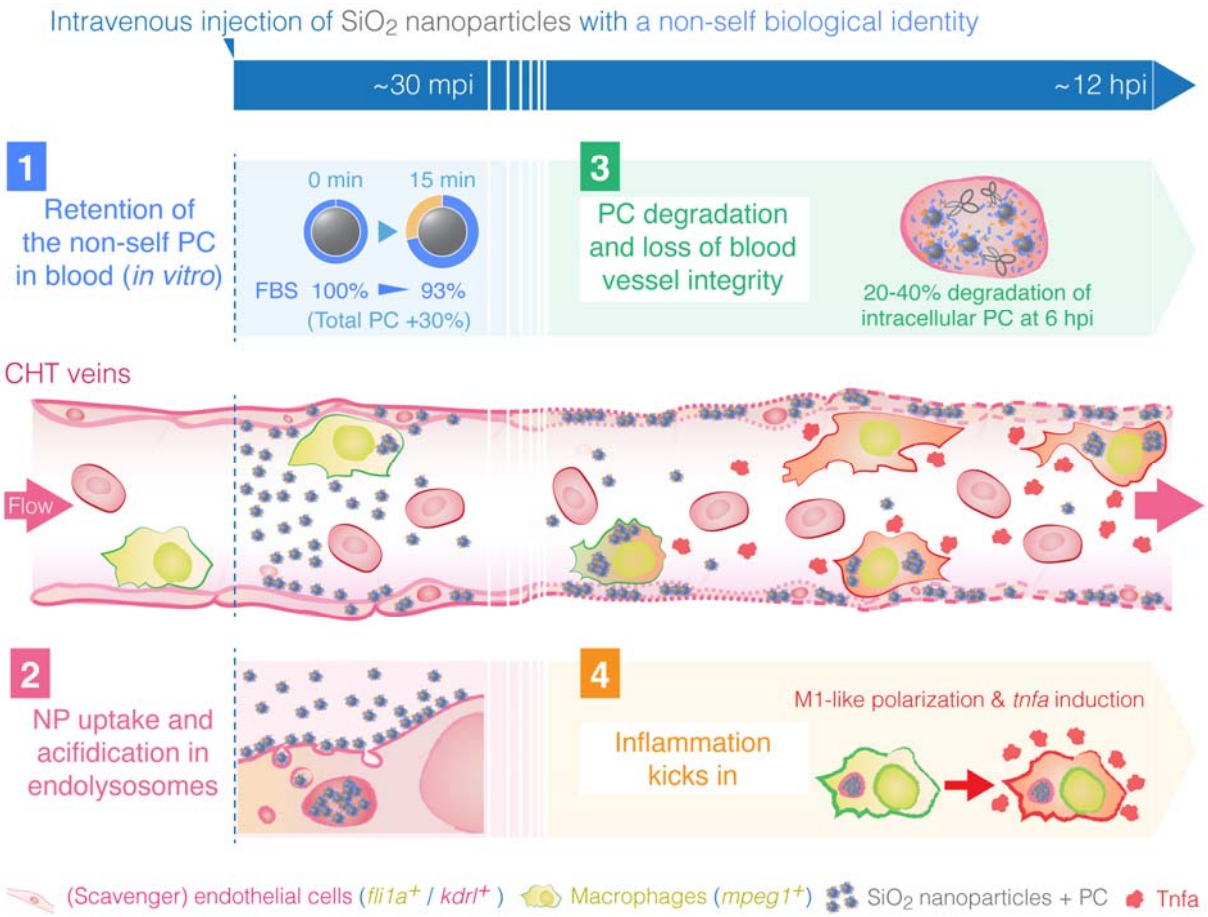

Figure 6. Schematic illustrating four elements directing the biological fate of nanoparticles with a non-self biological identity. SiO_2 nanoparticles may retain the pre-formed FBS PC as a non-self biological identity even after exposure to zebrafish blood plasma, however, with additional proteins that have a high affinity for the nanoparticles (**1**). Within 30 min following IV injections, FBS PC nanoparticles are rapid sequestered by scavenger ECs and acidified in the endolysosomal compartments (**2**). In a longer time-frame, degradation of the FBS PC occurs around 4-6 hpi in both scavenger ECs and macrophages while the former loses its integrity (**3**). Concurrently, macrophages are activated to an inflammatory phenotype (M1-like polarization) that secretes the cytokine Tnfa coordinating the onset of inflammation (**4**).

Methods

Preparation and characterization of FBS PC nanoparticles. Fluorescently-labelled 70 nm SiO_2 nanoparticles (plain, carboxyl and amine surfaces) were purchased from micromod Partikeltechnologie GmbH (Germany) and characterized as described previously[14,25]. Heat-inactivated FBS (ThermoFisher Scientific) was centrifuged at 16,000*g* for 3 min to remove any insoluble aggregates and the supernatant was mixed with nanoparticles at final concentrations of 90% (v/v) FBS and 0.4 mg/ml nanoparticles. Following 2 h incubation in darkness at 37°C, the nanoparticle-protein complexes were pelleted by centrifugation (20,000*g*, 20 min), PBS-washed three times, and redispersed in PBS at a nominal concentration of 4 mg/ml. The actual concentration was adjusted by fluorimetry using pristine nanoparticles as the reference on a LS55 luminescence spectrometer (Perkin Elmer), where necessary, after direct labelling of PC as described below. The endotoxin level of FBS PC nanoparticles was tested using a Pierce LAL Chromogenic Endotoxin Quantitation kit (ThermoFisher Scientific) and was 1.85 ± 0.07 EU/ml (mean ± S.D. of two independently prepared batches). The mass of proteins on nanoparticles was directly quantified using a Pierce BCA Protein Assay kit (ThermoFisher Scientific) with an additional centrifugation step (20,000*g*, 30 min) to collect the nanoparticle-free supernatant for absorbance measurements using a Varioscan plate reader (ThermoFisher Scientific). For TEM, specimens for Pristine and FBS PC nanoparticles were prepared as previously described[14] except that for negative staining uranyl formate was used instead of uranyl acetate.

Fluorescence labelling of proteins. Proteins were in all cases labelled *via* the amine-reactive crosslinker N-hydroxysuccinimide (NHS) esters, available as water soluble Sulpho-Cyanine 5 or Sulpho-Cyanine 3 NHS esters (Lumiprobe), or pHrodo Red NHS esters (ThermoFisher Scientific). For direct conjugation to corona proteins, 0.05 mg/ml of each dye (singly or as a mixture of Cyanine 5 and pHrodo Red) were incubated with FBS PC nanoparticles for 2 h at room temperature (RT, 21°C). The reaction was quenched by 50 mM Tris, followed by PBS washing (20,000*g*, 20 min, three times centrifugation) to remove the free dyes. Free proteins labelled following the

manufacturer's instructions were purified using Sephadex G-25 in PD-10 Desalting Columns (GE Healthcare Life Sciences).

PC retention experiments *in vitro*. Collection of zebrafish blood plasma (DrBP) is described in full details in our earlier report[14]. As DrBP obtained from adult female fish contains the yolk precursor proteins vitellogenins[14], for this study only male fish were chosen for the blood collection. To study the hard corona compositions, nanoparticles with FBS PC or DrBP PC (0.4 mg/ml) were washed by centrifugation (three times in PBS, 20,000*g*, 20 min) for SDS-PAGE. For the PC retention experiments, DrBP was Cy3-labelled as free proteins. Cy5-labelled FBS PC nanoparticles (0.2 mg/ml) were incubated with 1 mg/ml Cy3-labelled DrBP (or only in PBS for a control) at 28°C (physiological temperature for zebrafish) in the dark for 15 min or 6 h, before proceeding to the centrifugation-based isolation for fluorimetry and SDS-PAGE. Protein mass was calculated based on known protein concentrations (BCA assays directly on FBS PC or on free FBS proteins) and fluorescence measurements by fluorimetry using reference pristine nanoparticles (to estimate nanoparticle concentrations) and free FBS-Cy3 proteins (to estimate the mass of DrBP proteins added to PC). Subsequently, for SDS-PAGE, proteins bound to the nanoparticles were stripped by boiling for 5 min after addition of 5× concentrated reducing sample buffer (5 % SDS, 50% glycerol, 100 mM DTT in 0.3 M Tris). The nanoparticle-free supernatant after centrifugation (20,000*g*, 30 min) was loaded on a Bolt 4-12% Bis-Tris Plus Gel at the volume corresponding to 150 µg or 30 µg nanoparticles in the original samples and run by electrophoresis at 160 V. For fluorescence scans, the gels were first imaged by an Amersham Typhoon NIR laser scanner (GE Healthcare Life Sciences). Subsequently, protein bands were stained by Coomassie brilliant blue (Imperial Protein Stain; ThermoFisher Scientific) and scanned on a Bio-Rad gel documentation system. Band intensity quantification was performed using the plot profile tool in Fiji/ImageJ[47,48]. Three independent experiments were performed for SDS-PAGE and representative results are shown.

Fluorescence measurements at intracellular pH. The fluorescence intensity of Pristine nanoparticles, free proteins-labelled with dyes, and their complexes (FBS PC nanoparticles) at pH relevant for intracellular environments was measured in phosphate-citrate buffer by fluorimetry as above. The nanoparticles did not show any signs of agglomeration between the pH range from 4.0 to 7.4, as determined by DLS.

Protein identification on excised bands. In-gel digestion of selected proteins was performed essentially as described previously[49]. The tryptic peptides were micro-purified using C18 stage tips (Proxeon, ThermoScientific). Nano-electrospray ionization MS/MS (nanoESI-MS/MS) analyses were performed on an EASY-nLC II system (ThermoScientific) connected to a TripleTOF 5600+ mass spectrometer (AB SCIEX) equipped with a NanoSpray III source (AB SCIEX) operated under Analyst TF 1.6 control. The trypsin-digested samples were suspended in 0.1% formic acid, injected, trapped and desalted isocratically on a precolumn (ReproSil-Pur C18-AQ 3 μm resin, Dr. Maisch GmbH, Germany). The peptides were eluted and separated on a 15 cm analytical column (75 μm i.d.), pulled in-house (P2000 laser puller, Sutter Instrument), and packed with ReproSil-Pur C18-AQ 3 μm resin (Dr. Maisch GmbH, Germany). Peptides were eluted from the analytical column at a flow rate of 250 nl/min using a 30 min gradient from 5% to 35% of solution B (0.1% formic acid, 100% acetonitrile). The collected MS files were converted to Mascot generic format (MGF) using the AB SCIEX MS Data Converter beta 1.1 (AB SCIEX) and the "protein pilot MGF" parameters. The generated peak lists were searched using an in- house Mascot search engine (Matrix Science). Search parameters were allowing one missed trypsin cleavage site and propionamide as a fixed modification with peptide tolerance and MS/MS tolerance set to 20 ppm and 0.4 Da, respectively.

Zebrafish. Zebrafish (*Danio rerio*) were bred and maintained in accordance with the Danish legislation. Experiments were performed on 3 dpf embryos from a wild-type strain (AB) or established transgenic lines; *Tg(fli1a:EGFP)*^{y1} and *Tg(kdrl:hsa.HRAS-mCherry)*^{s916} or *Tg(kdrl:mCherry-F)* for short were used as reporter lines for endothelial cells[50-52];

Tg(mpeg1:mCherry)^{gl23} for embryonic macrophages[53]; *Tg(tnfa:GFP-F)*^{ump5} for transcriptional activation of *tnfa*[53].

Intravital confocal laser scanning microscopy and image analysis. In the same manner as described previously[25], anesthetized zebrafish embryos (3 dpf) were embedded in 0.8% (w/v) low-melting point agarose for IV microinjection with nominal 10 ng (3×10^7 particles, 3 nl at 3.4 mg/ml) of nanoparticles along with sterile-filtered, endotoxin-free phenol red solution in DPBS (0.5% w/v, BioReagent; Sigma-Aldrich) as a loading dye/buffer. As a vehicle control, water (MilliQ, 18.2 MΩ) was used likewise diluted in the loading buffer. The injection dose of free FBS proteins was 2 ng, equivalent to the measured protein mass of FBS PC nanoparticles. For M1-like polarization of macrophages, as previously performed[25], γ-irradiated LPS from *Escherichia coli* O111:B4 (BioXtra; Sigma-Aldrich) dissolved in PBS was IV injected at the dose of 2.4 ng, which is 1,000,000-fold higher than the measured endotoxin level detected in FBS PC nanoparticles. Injected embryos were observed under a Zeiss LSM 780 upright confocal microscope (Carl Zeiss) with lasers at 405 nm (Pacific Blue), 488 nm (GFP/EGFP/FITC), 568 nm (mCherry, pHrodo Red), and 633 nm (Cy5). Objective lenses used were EC Plan-Neofluar 10x/0.3 M27 for tile scanning of the whole embryo and W Plan-Apochromat 40×/1.0 DIC M27 (Carl Zeiss) for live imaging. All images were acquired as 2-µm optical sections to construct z-stack images and presented as the maximum intensity z-stack projections using Fiji/ImageJ[47,48]. Detailed descriptions of the 3D mask approach and image analysis method are fully presented in our previous report[25]. Similarly to "sequestered nanoparticles" defined therein, "sequestered PC" was defined by thresholding of the PC signals at >20 times higher than the noise level typically picking only the immobilized clusters associated with cells. Likewise, "Total FI" is defined by mean FI multiplied by area (μm^2) after thresholding to remove the background noise signals. As pre-processing of the stacked images for calculating the pixel-by-pixel fluorescence ratios, a value of 1 was assigned to all pixels in both fluorescence channels before applying a 3D mask specific for FBS PC (Fig. 3, FBS-Cy5 as the mask for FBS-pHrodo) or nanoparticles (Fig. 4, NP-Pacific Blue as the mask for FBS-Cy5). The stacked images

were then processed as maximum intensity z-projections and the fluorescence ratio of two channels was calculated in the image using a 32-bit floating point mode. The resulting values were multiplied by a factor of 10,000 to convert the images back to the 16-bit range (0-65535), where the value of 10,000 equals to the fluorescence ratio of 1. To obtain a representative value for the fluorescence ratios, the median, rather than the mean, is reported. All imaging experiments were repeated independently at least once more to confirm the reproducibility.

Kinetic models and statistics. Non-linear curve fitting was performed in R (ver. 3.5.1) for results obtained from time-lapse imaging. All individual data points were fitted using an exponential decay model; $y = y_f + (y_0 - y_f)e^{-\lambda t}$, where the measured value y starts at y_0 and decreases towards y_f as an exponential function of time t with the rate constant λ, or logistic/Gompertz models; $y = y_f \times \frac{y_0}{(y_f - y_0)e^{-\lambda t} + y_0}$ and $y = y_f \times \left(\frac{y_0}{y_f}\right) e^{-\lambda t}$, where the starting value y_0 grows towards the plateau y_f as an exponential function of time t with the rate constant λ. The fitted parameters are shown in Supplementary Table 2. For parametric statistics, the input data were log-transformed to satisfy the assumption of normality. One-way analysis of variance (ANOVA) with Tukey's HSD post-hoc comparisons were performed in R (ver. 3.5.1) following Levene's test on the homogeneity of variances. Significant differences between the tested populations were determined as $\alpha = 0.05$.

Transmission electron microscopy. As described previously[25], injected embryos (30 mpi) were cooled on ice for 10 min and fixed with the modified Karnovsky fixative for 80 min during which the embryos were retrieved from agarose. The head of the fixed embryos was then removed for better penetration of the fixative and kept overnight at 4°C. The embryos were washed twice with 0.1 M cacodylate buffer (pH 7.0) and post-fixed with secondary fixative (1% w/v OsO_4, 0.1 M cacodylate buffer, pH 7.0) for 1 h on ice. The fixed embryos were thoroughly washed in H_2O and contrasted with 1% (w/v) uranyl acetate solution for 1-2 h at 4°C in the dark. For embedding into EPON 812 resin, the fixed embryos were thoroughly washed in H_2O, dehydrated and mounted through steps consisting of a series of ethanol (50%-70%-90%-99%) and a 1,2-propylene

oxide:EPON mixture (1:0-1:1-0:1). Several sagittal sections were prepared using a glass knife and stained by toluidine blue O to help approximate the position of the CVP before ultra-microtome sectioning. Serial ultrathin sections ("silver" 50-60 nm thick) were then cut with a Leica EM UC7 ultramicrotome (Leica Microsystems) mounted with a diamond knife (Ultra 45°; DiATOME, PA, USA). Sections were placed on a formvar/carbon-supported copper slot grid and stained with saturated uranyl acetate and Reynold's lead citrate solution. The specimens were examined under a Tecnai G2 Spirit TEM (FEI company, ThermoFisher Scientific) operating at 120 KeV.

Acknowledgements

This work was financially supported by the grants R219-2016-327 and R324-2019-1644 from Lundbeck Foundation (Y.H.), the grant DFF-4181-00473 from Independent Research Fund Denmark | the Research Council for Natural Sciences (FNU) and the center grant CellPAT (DNRF135) from the Danish National Research Foundation Center (H.M-B. and D.S.S.). We gratefully acknowledge P. Engelmann from the University of Pécs, Hungary, for his advice on the manuscript. We also thank the fish facility at Aarhus University for zebrafish husbandry.

Author contributions

H.M-B. and Y.H. conceived the project. H.M-B. prepared and characterized nanoparticles with pre-formed PC. C.S. and J.J.E. performed tandem mass spectrometry analysis. P.B.J. and T.B. prepared specimens for TEM. K.K.S. and C.O. provided conceptual advice on the zebrafish model. D.S.S. and Y.H. supervised the project. Y.H. designed, performed and analyzed all imaging experiments and wrote the manuscript.

Competing financial interests

The authors declare no competing financial interests.

References

1 Rodriguez, P. L. *et al.* Minimal "Self" Peptides That Inhibit Phagocytic Clearance and Enhance Delivery of Nanoparticles. *Science* **339**, 971, (2013).

2 Parodi, A. *et al.* Synthetic nanoparticles functionalized with biomimetic leukocyte membranes possess cell-like functions. *Nat. Nanotechnol.* **8**, 61-68, (2013).

3 Corbo, C. *et al.* Unveiling the in Vivo Protein Corona of Circulating Leukocyte-like Carriers. *ACS Nano* **11**, 3262-3273, (2017).

4 Hadjidemetriou, M., Al-Ahmady, Z. & Kostarelos, K. Time-evolution of in vivo protein corona onto blood-circulating PEGylated liposomal doxorubicin (DOXIL) nanoparticles. *Nanoscale* **8**, 6948-6957, (2016).

5 Hadjidemetriou, M. *et al.* In Vivo Biomolecule Corona around Blood-Circulating, Clinically Used and Antibody-Targeted Lipid Bilayer Nanoscale Vesicles. *ACS Nano* **9**, 8142-8156, (2015).

6 Hadjidemetriou, M. *et al.* The Human In Vivo Biomolecule Corona onto PEGylated Liposomes: A Proof-of-Concept Clinical Study. *Adv. Mater.* **31**, 1803335, (2019).

7 Mortimer, G. M. *et al.* Cryptic Epitopes of Albumin Determine Mononuclear Phagocyte System Clearance of Nanomaterials. *ACS Nano* **8**, 3357-3366, (2014).

8 Deng, Z. J., Liang, M., Monteiro, M., Toth, I. & Minchin, R. F. Nanoparticle-induced unfolding of fibrinogen promotes Mac-1 receptor activation and inflammation. *Nat. Nanotechnol.* **6**, 39-44, (2011).

9 Medzhitov, R. & Janeway, C. A. Decoding the Patterns of Self and Nonself by the Innate Immune System. *Science* **296**, 298, (2002).

10 Bros, M. *et al.* The Protein Corona as a Confounding Variable of Nanoparticle-Mediated Targeted Vaccine Delivery. *Front. Immunol.* **9**, 1760, (2018).

11 Pisani, C. *et al.* The species origin of the serum in the culture medium influences the in vitro toxicity of silica nanoparticles to HepG2 cells. *PLoS One* **12**, e0182906, (2017).

12 Schöttler, S., Klein, K., Landfester, K. & Mailänder, V. Protein source and choice of anticoagulant decisively affect nanoparticle protein corona and cellular uptake. *Nanoscale* **8**, 5526-5536, (2016).

13 Albanese, A. *et al.* Secreted Biomolecules Alter the Biological Identity and Cellular Interactions of Nanoparticles. *ACS Nano* **8**, 5515-5526, (2014).

14 Hayashi, Y. *et al.* Female *versus* male biological identities of nanoparticles determine the interaction with immune cells in fish. *Environ. Sci. Nano* **4**, 895-906, (2017).

15 Askes, S. H. C. *et al.* Dynamics of dual-fluorescent polymersomes with durable integrity in living cancer cells and zebrafish embryos. *Biomaterials* **168**, 54-63, (2018).

16 Campbell, F. *et al.* Directing Nanoparticle Biodistribution through Evasion and Exploitation of Stab2-Dependent Nanoparticle Uptake. *ACS Nano* **12**, 2138-2150, (2018).

17 Sieber, S. *et al.* Zebrafish as a preclinical in vivo screening model for nanomedicines. *Adv. Drug Delivery Rev.* **151-152**, 152-168, (2019).

18 Sieber, S. *et al.* Zebrafish as an early stage screening tool to study the systemic circulation of nanoparticulate drug delivery systems in vivo. *J. Controlled Release* **264**, 180-191, (2017).

19 Sieber, S. *et al.* Zebrafish as a predictive screening model to assess macrophage clearance of liposomes in vivo. *Nanomed. Nanotech. Biol. Med.* **17**, 82-93, (2019).

20 Le, D. *et al.* Straightforward access to biocompatible poly(2-oxazoline)-coated nanomaterials by polymerization-induced self-assembly. *Chem. Commun. (Camb.)* **55**, 3741-3744, (2019).

21 Mane, S. R. *et al.* Intrinsically Fluorescent, Stealth Polypyrazoline Nanoparticles with Large Stokes Shift for In Vivo Imaging. *Small* **14**, 1801571, (2018).

22 Dal, N.-J. K. *et al.* Zebrafish Embryos Allow Prediction of Nanoparticle Circulation Times in Mice and Facilitate Quantification of Nanoparticle–Cell Interactions. *Small* **16**, 1906719, (2020).

23 Evensen, L. *et al.* Zebrafish as a model system for characterization of nanoparticles against cancer. *Nanoscale* **8**, 862-877, (2016).

24 Fenaroli, F. *et al.* Enhanced Permeability and Retention-like Extravasation of Nanoparticles from the Vasculature into Tuberculosis Granulomas in Zebrafish and Mouse Models. *ACS Nano* **12**, 8646-8661, (2018).

25 Hayashi, Y. *et al.* Differential Nanoparticle Sequestration by Macrophages and Scavenger Endothelial Cells Visualized in Vivo in Real-Time and at Ultrastructural Resolution. *ACS Nano* **14**, 1665-1681, (2020).

26 Yu, T., Hubbard, D., Ray, A. & Ghandehari, H. *In vivo* biodistribution and pharmacokinetics of silica nanoparticles as a function of geometry, porosity and surface characteristics. *J. Controlled Release* **163**, 46-54, (2012).

27 Tenzer, S. *et al.* Rapid formation of plasma protein corona critically affects nanoparticle pathophysiology. *Nat. Nanotechnol.* **8**, 772-781, (2013).

28 Babaei, F. *et al.* Novel Blood Collection Method Allows Plasma Proteome Analysis from Single Zebrafish. *J. Proteome Res.* **12**, 1580-1590, (2013).

29 Lucitt, M. B. *et al.* Analysis of the Zebrafish Proteome during Embryonic Development. *Molecular & Cellular Proteomics* **7**, 981, (2008).

30 Li, C., Tan, X. F., Lim, T. K., Lin, Q. & Gong, Z. Comprehensive and quantitative proteomic analyses of zebrafish plasma reveals conserved protein profiles between genders and between zebrafish and human. *Sci. Rep.* **6**, 24329, (2016).

31 Chen, F. *et al.* Complement proteins bind to nanoparticle protein corona and undergo dynamic exchange in vivo. *Nat. Nanotechnol.* **12**, 387-393, (2017).

32 Cohen, J. D., Thompson, S. & Ting, A. Y. Structure-Guided Engineering of a Pacific Blue Fluorophore Ligase for Specific Protein Imaging in Living Cells. *Biochemistry (Mosc.)* **50**, 8221-8225, (2011).

33 Casey, J. R., Grinstein, S. & Orlowski, J. Sensors and regulators of intracellular pH. *Nat. Rev. Mol. Cell Biol.* **11**, 50, (2009).

34 Steinberg, B. E. *et al.* A cation counterflux supports lysosomal acidification. *J. Cell Biol.* **189**, 1171-1186, (2010).

35 Neiss, W. F. The electron density of light and dark lysosomes in the proximal convoluted tubule of the rat kidney. *Histochemistry* **77**, 63-77, (1983).

36 Soo Choi, H. *et al.* Renal clearance of quantum dots. *Nat. Biotechnol.* **25**, 1165-1170, (2007).

37 Wang, F. *et al.* The biomolecular corona is retained during nanoparticle uptake and protects the cells from the damage induced by cationic nanoparticles until degraded in the lysosomes. *Nanomed. Nanotech. Biol. Med.* **9**, 1159-1168, (2013).

38 Bertoli, F., Garry, D., Monopoli, M. P., Salvati, A. & Dawson, K. A. The Intracellular Destiny of the Protein Corona: A Study on its Cellular Internalization and Evolution. *ACS Nano* **10**, 10471-10479, (2016).

39 Nguyen-Chi, M. *et al.* Identification of polarized macrophage subsets in zebrafish. *eLife* **4**, e07288, (2015).

40 Westman, J., Grinstein, S. & Marques, P. E. Phagocytosis of Necrotic Debris at Sites of Injury and Inflammation. *Front. Immunol.* **10**, 3030, (2020).

41 Verweij, F. J. *et al.* Live Tracking of Inter-organ Communication by Endogenous Exosomes In Vivo. *Dev. Cell* **48**, 573-589.e574, (2019).

42 Sepulcre, M. P. *et al.* Evolution of Lipopolysaccharide (LPS) Recognition and Signaling: Fish TLR4 Does Not Recognize LPS and Negatively Regulates NF-κB Activation. *The Journal of Immunology* **182**, 1836, (2009).

43 van der Vaart, M., van Soest, J. J., Spaink, H. P. & Meijer, A. H. Functional analysis of a zebrafish *myd88* mutant identifies key transcriptional components of the innate immune system. *Disease Models & Mechanisms* **6**, 841, (2013).

44 Bianchi, M. E. *et al*. High-mobility group box 1 protein orchestrates responses to tissue damage via inflammation, innate and adaptive immunity, and tissue repair. *Immunol. Rev*. **280**, 74-82, (2017).

45 Rock, K. L. & Kono, H. The Inflammatory Response to Cell Death. *Annu. Rev. Pathol.: Mech. Dis*. **3**, 99-126, (2008).

46 Walczyk, D., Bombelli, F. B., Monopoli, M. P., Lynch, I. & Dawson, K. A. What the Cell "Sees" in Bionanoscience. *J. Am. Chem. Soc.* **132**, 5761-5768, (2010).

47 Schindelin, J. *et al.* Fiji: an open-source platform for biological-image analysis. *Nat. Methods* **9**, 676-682, (2012).

48 Schneider, C. A., Rasband, W. S. & Eliceiri, K. W. NIH Image to ImageJ: 25 years of image analysis. *Nat. Methods* **9**, 671-675, (2012).

49 Hayashi, Y. *et al.* Species Differences Take Shape at Nanoparticles: Protein Corona Made of the Native Repertoire Assists Cellular Interaction. *Environ. Sci. Technol.* **47**, 14367-14375, (2013).

50 Hogan, B. M. *et al*. ccbe1 is required for embryonic lymphangiogenesis and venous sprouting. *Nat. Genet*. **41**, 396-398, (2009).

51 Lawson, N. D. & Weinstein, B. M. In Vivo Imaging of Embryonic Vascular Development Using Transgenic Zebrafish. *Dev. Biol*. **248**, 307-318, (2002).

52 Chi, N. C. *et al*. Foxn4 directly regulates tbx2b expression and atrioventricular canal formation. *Genes Dev.* **22**, 734-739, (2008).

53 Ellett, F., Pase, L., Hayman, J. W., Andrianopoulos, A. & Lieschke, G. J. mpeg1 promoter transgenes direct macrophage-lineage expression in zebrafish. *Blood* **117**, e49-e56, (2011).